

ActiveInitSplat: How Active Image Selection Helps Gaussian Splatting

Konstantinos D. Polyzos^{1*}, Athanasios Bacharis^{2*}, Saketh Madhuvarasu¹,
Nikos Papanikolopoulos², Tara Javidi¹

¹ University of California San Diego ² University of Minnesota

* Authors declare equal contribution

Abstract

Gaussian splatting (GS) along with its extensions and variants provides outstanding performance in real-time scene rendering while meeting reduced storage demands and computational efficiency. While the selection of 2D images capturing the scene of interest is crucial for the proper initialization and training of GS, hence markedly affecting the rendering performance, prior works rely on passively and typically densely selected 2D images. In contrast, this paper proposes ‘ActiveInitSplat’, a novel framework for active selection of training images for proper initialization and training of GS. ActiveInitSplat relies on density and occupancy criteria of the resultant 3D scene representation from the selected 2D images, to ensure that the latter are captured from diverse viewpoints leading to better scene coverage and that the initialized Gaussian functions are well aligned with the actual 3D structure. Numerical tests on well-known simulated and real environments demonstrate the merits of ActiveInitSplat resulting in significant GS rendering performance improvement over passive GS baselines, in the widely adopted LPIPS, SSIM, and PSNR metrics.

1. Introduction

3D scene representation and novel view synthesis are fundamental tasks in computer vision with diverse applications including autonomous driving, robotics, and medical imaging just to name a few. The goal in these tasks is to develop models capable of fast scene rendering while maintaining high visual quality, minimizing storage requirements, and ensuring computational efficiency. Gaussian splatting (GS), first proposed in [12], along with its extended variants have sparked attention in the research community due to their efficient 3D scene representation via a set of anisotropic Gaussian functions, allowing for fast rendering with memory efficiency, and outstanding visual performance.

Across different GS models, the selection of initial train-

ing images is known to be a crucial factor for the rendering performance, since they have a direct impact on the initialization and training of GS. However, existing GS frameworks hinge on a *passively* pre-selected and typically dense set of training images which ensures redundancy, along with increased processing and computational cost. Even in the few GS frameworks designed for efficient rendering with a limited number of images, passive selection may confine the expressiveness of the 3D scene representation, potentially leading to reduced scene coverage. This paper, in contrast, provides a general framework for *active* and strategic selection of a few yet informative training images captured at diverse viewpoints, to ensure effective GS rendering performance at a lower sampling cost.

While the idea of actively optimizing the training set of images seems natural and necessary, identifying a compact set of optimal camera views that lead to high-quality 3D scene representation, is fundamentally challenged by the need to guarantee diverse viewpoints without incurring redundancy. Specifically, (i) there is no explicit function in the existing literature that maps a certain set of images to the quality of the reconstructed 3D scene and, consequently, to GS rendering performance; (ii) even if such an explicit function were provided, it certainly would depend on the structure of the scene for which prior information is typically not available; and finally (iii) a sequential processing of multiple different sets of images to empirically assess GS rendering performance is impractical. In the face of these challenges, this paper proposes ‘ActiveInitSplat’, a novel active GS framework shown in Fig. 1, whose contributions can be summarized in the following aspects.

- In contrast to existing passive GS approaches, ActiveInitSplat is the first work to introduce an effective and lightweight active camera view selection strategy for Gaussian Splatting without requiring any depth information or any prior knowledge (such as geometric cues) of the 3D scene of interest.
- To guide the active selection process, ActiveInitSplat proposes an innovative optimization formulation, where the objective function integrates density- and occupancy-

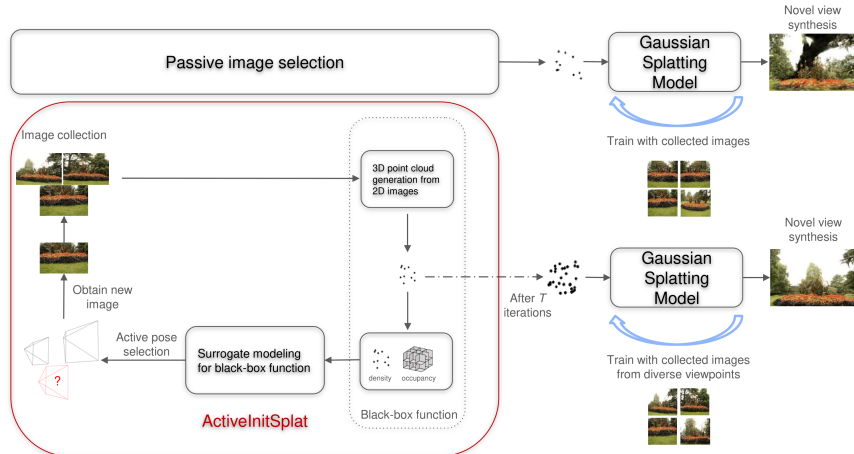


Figure 1. **ActiveInitSplat in a nutshell.** In contrast to existing Gaussian splatting (GS) methods that rely on passively (and possibly densely) collected 2D images of the scene of interest, ActiveInitSplat actively selects informative images to assist the initialization and training of GS. The active selection mechanism lies on optimizing a (black-box) function quantifying the quality of the resultant 3D point cloud from the selected images via density and occupancy criteria. The collected images are captured from diverse viewpoints, ensuring better scene coverage and facilitating the accurate alignment of the initialized Gaussian functions with the underlying 3D structure.

based criteria of the 3D point cloud, informing the initialization step in GS. As such, our method is agnostic to the subsequent steps of GS. Hence, it can be readily incorporated into the growingly extended variants of GS architectures.

- Numerical tests on simulated and well-known real-world benchmark 3D scenes, demonstrate the significance of ActiveInitSplat in actively capturing informative training images from diverse viewpoints for GS, with substantial rendering performance improvement compared to passive selection counterparts.
- The proposed active selection mechanism is shown to benefit GS models both in sparse- and dense-view regimes. In addition, ActiveInitSplat performs well both in the general setting of selecting optimal images from any position in 3D space, as well as in scenarios where the view selection is limited to a finite set of images (such as benchmark datasets).

2. Related Works

In this section, prior art is presented to contextualize the motivation and contributions of ActiveInitSplat.

2.1. Novel view synthesis and scene rendering

Novel view synthesis (NVS) refers to the problem of estimating views of a 3D scene of interest at unobserved viewpoints/poses based on a certain budget of observed images. NVS initially garnered notable attention with the emergence of approaches leveraging the SfM process, which estimates a (typically sparse) 3D scene representation, and multi-view

stereo (MVS) techniques that enable denser 3D reconstructions; see e.g. [3, 13]. Albeit interesting, the visual quality of the rendered images admitted further improvements. Recently, neural radiance field (NeRF) based methods that leverage multi-layer perceptrons (MLPs) utilizing volumetric ray-marching for NVS, have shown great empirical success. For example, the ‘Mip-NeRF360’ framework in [1] has achieved outstanding visual quality of rendered images but may entail up to 48 hours of training, which discourages its application in time-sensitive tasks. To alleviate such computational burdens, existing NeRF-based methods employ simpler MLPs or other techniques; see e.g. [4, 20, 27]. Although being more efficient in terms of training, these approaches show inferior rendering quality compared to ‘Mip-NeRF360’.

2.2. Gaussian splatting for novel view synthesis

Striving for high rendering quality and reduced training time compared to the ‘Mip-NeRF360’ NeRF-based approach, the recently developed Gaussian splatting (GS) methods provide principled frameworks to represent a 3D scene of interest using a set of Gaussian functions. To initialize these Gaussian functions so that they are aligned with the 3D structure, the initial GS approach in [12] relies on the SfM process to obtain a representation of the 3D scene. Yet, the SfM process may become inefficient when the number of training images is large, may introduce accumulated errors in the rendering process, and necessitates explicit camera pose knowledge [7]. To cope with the latter challenge, alternative pose-free GS approaches have been proposed in [8, 10] that rely on monocular depth estimation for 3D rep-

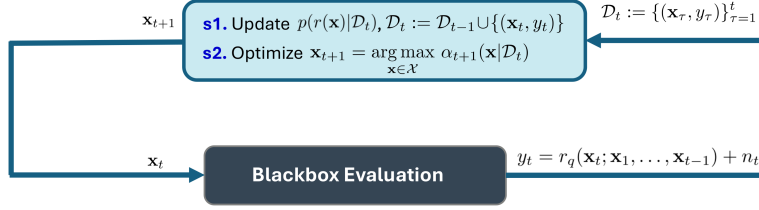


Figure 2. Active viewpoint selection process using Gaussian process-based surrogate modeling for black-box optimization.

resentation instead of SfM. However, they may still require extensive training time. Aiming at efficient training solutions, existing SfM-free GS methods [7, 23] capitalize on pre-trained models, including ‘DUSt3R’ [29] and its following ‘MASt3R’ [14], that provide geometry priors for densely sampled, pixel-aligned stereo points. Besides leveraging prior models, alternative SfM-free approaches have been proposed for NVS with efficiency; see e.g. [26, 30–32]. In all these approaches, the selection of the initial set of training images plays a significant role in the rendering performance. Despite their well-documented merits, all these approaches rely on a passively (and possibly densely) pre-selected set of training images, which may lead to redundant views along with less expressive scene representation and reduced scene coverage, hence motivating the need for active camera view selection to aid GS.

Lying at the crossroads of robotics and computer vision, existing approaches including [11, 15] combine GS models with additional supervision from Voronoi graphs or voxel maps for active path planning, while others leverage GS-based scene representations for active mapping [5]. Here, we would like to emphasize that these prior works that integrate GS solutions in active mapping or active high-fidelity scene reconstruction for various robotic applications are distinct from the proposed ActiveInitSplat in the sense that the latter aims to find informative camera views for GS beforehand without need for incremental re-training and use of GS. In robotics settings, the recent work in [25] seeks instructive camera views for GS accounting for depth uncertainty-based criteria. Albeit interesting, it is tailored for robotic environments where the targeted scene is mainly focused on specific objects without showing generalizability to broader 3D scenes of interest. In addition, the proposed framework in [25] integrates ground-truth depth information from depth sensors, which may not be given in several practical settings. Identifying informative camera views for any 3D scene of interest beforehand without the need for re-training of GS during the selection process, and without need for any depth or prior scene information is still unexplored.

3. Preliminaries and Problem Formulation

The key concept of GS is to model a 3D scene of interest using a set of N anisotropic Gaussian functions $\{G_i\}_{i=1}^N$ [12]. Relying on an initial set of T pre-selected training images or camera views $\{\mathbf{I}_\tau\}_{\tau=1}^T$ at viewpoints $\{\mathbf{x}_\tau\}_{\tau=1}^T$, conventional GS starts with an (possibly sparse) initial 3D scene representation expressed by a set of 3D points called point cloud (PC), that is typically captured by the SfM process [22]. It is worth noticing that there exist alternative multi-view stereo reconstruction methods for 3D PC prediction that can be used, which aim to overcome the limitations of the traditional SfM process (c.f. Sec. 2).

For each point $\mathbf{p}_i, i \in \{1, \dots, N\}$ in the PC, a Gaussian function is defined as

$$G_i(\mathbf{z}) = \alpha_i \exp\left(-\frac{1}{2}(\mathbf{z} - \mathbf{m}_i)^\top \boldsymbol{\Sigma}_i^{-1}(\mathbf{z} - \mathbf{m}_i)\right) \quad (1)$$

where \mathbf{z} represents any point in the 3D space that the Gaussian function is evaluated, \mathbf{m}_i is the mean of Gaussian G_i initially centered at the 3D location of \mathbf{p}_i , $\boldsymbol{\Sigma}_i$ is the 3×3 covariance matrix that determines the shape, size and orientation of G_i , and α_i is the opacity that indicates the contribution of G_i to the final rendered images. Relying on these Gaussian functions, the 2D image rendering formula is [12]

$$\mathbf{c}(\mathbf{p}) = \sum_{i=1}^N \mathbf{c}_i G_i^{2D}(\mathbf{p}) \prod_{j=1}^{i-1} (1 - G_j^{2D}(\mathbf{p})) \quad (2)$$

where $\mathbf{c}(\mathbf{p})$ represents the color at any pixel \mathbf{p} in the rendered image and \mathbf{c}_i the color corresponding to the i th Gaussian that is either expressed via RGB values or spherical harmonics (SH) which are used to model view-dependent color variations. The function $G_i^{2D}(\cdot)$ denotes the projected 2D Gaussian function with mean and covariance given by

$$\mathbf{m}_i^{2D} = [u/b, l/b]^\top, [u, l, z]^\top = \mathbf{LW}[\mathbf{m}_i, 1]^\top \quad (3a)$$

$$\boldsymbol{\Sigma}_i^{2D} = \mathbf{JW}\boldsymbol{\Sigma}_i\mathbf{W}^\top\mathbf{J}^\top \quad (3b)$$

where matrices \mathbf{L} , \mathbf{W} contain intrinsic and extrinsic camera parameters respectively, and \mathbf{J} is the Jacobian matrix.

All Gaussian parameters are trained so that the rendered images match the corresponding training ground-truth ones; i.e. $\{\mathbf{I}_\tau\}_{\tau=1}^T$. To ensure that the covariance matrix $\boldsymbol{\Sigma}_i$ of each Gaussian i remains positive semi-definite

during the optimization process, it is decomposed as $\Sigma_i = \mathbf{R}_i \mathbf{S}_i \mathbf{S}_i^\top \mathbf{R}_i^\top$ where \mathbf{R}_i is the 3×3 diagonal scaling matrix and \mathbf{S}_i represents the rotation matrix analytically expressed in quaternions. The selection of the initial set of camera poses $\{\mathbf{x}_\tau\}_{\tau=1}^T$ that provide the initial training images $\{\mathbf{I}_\tau\}_{\tau=1}^T$, is critical for the GS performance since they affect the initialization and training of GS. Nonetheless, the optimal selection of initial camera poses is a non-trivial task and thus most existing works rely on *passive* selection of training images. In the next section, we will outline our proposed method for *active* selection of informative camera poses $\{\mathbf{x}_\tau^*\}_{\tau=1}^T$ that can assist GS models.

4. Active Camera View Selection for GS

Aiming at actively identifying the most informative camera poses $\{\mathbf{x}_\tau^*\}_{\tau=1}^T$ used for proper initialization and training of GS, the present work introduces a novel optimization framework that relies on density and occupancy criteria of the PC in the 3D space emanating from the selected camera views. The intuition is that if the images from the actively selected camera poses result in more dense PCs with better scene coverage compared to passive selection, then (i) the initialized Gaussians will better cover the scene, avoiding missing areas or gaps and (ii) the training images will be selected from diverse viewpoints, thus facilitating the optimization process of GS.

At each slot t of the proposed active selection process, the goal is to select the optimal camera pose \mathbf{x}_t^* as

$$\mathbf{x}_t^* = \arg \max_{\mathbf{x} \in \mathcal{X}} r_q(\mathbf{x}; \mathbf{x}_1, \dots, \mathbf{x}_{t-1}) \quad (4)$$

where \mathcal{X} is the feasible set of candidate camera poses and $r_q(\cdot)$ is the objective function that evaluates the quality of the 3D scene representation leveraging density and occupancy-based criteria. Specifically, $r_q(\cdot)$ is expressed as

$$r_q(\mathbf{x}; \mathbf{x}_1, \dots, \mathbf{x}_{t-1}) := D(\mathcal{P}_C(\mathbf{x}; \mathbf{x}_1, \dots, \mathbf{x}_{t-1})) \cdot O(\mathcal{P}_C(\mathbf{x}; \mathbf{x}_1, \dots, \mathbf{x}_{t-1})) \quad (5)$$

where $\mathcal{P}_C(\mathbf{x}; \mathbf{x}_1, \dots, \mathbf{x}_{t-1})$ denotes the PC emanating from the images collected from camera poses $\{\mathbf{x}, \mathbf{x}_1, \dots, \mathbf{x}_{t-1}\}$. The density function $D(\mathcal{P}_C(\mathbf{x}; \mathbf{x}_1, \dots, \mathbf{x}_{t-1}))$ assesses the density of the PC by measuring the number of 3D points in the PC, and $O(\mathcal{P}_C(\mathbf{x}; \mathbf{x}_1, \dots, \mathbf{x}_{t-1}))$ quantifies the ‘‘occupancy’’ of the PC in the 3D space. Inspired by the notion of voxel maps [9, 19], where an environment of interest within a pre-defined bounding box can be represented by a set \mathcal{V} of non-overlapping 3D voxels, the occupancy function $O(\cdot)$ is explicitly defined as $O(\mathcal{P}_C(\mathbf{x}; \mathbf{x}_1, \dots, \mathbf{x}_{t-1})) = \sum_{i=1}^{|\mathcal{V}|} v_i / |\mathcal{V}|$, where $v_i = 1$ only if there is at least one 3D point in $\mathcal{P}_C(\mathbf{x}; \mathbf{x}_1, \dots, \mathbf{x}_{t-1})$ belonging to voxel i , and 0 otherwise.

The challenge in the optimization problem described in (4) is that the objective function $r_q(\cdot)$ cannot be expressed

analytically since there is no analytic expression for obtaining $\mathcal{P}_C(\mathbf{x}; \mathbf{x}_1, \dots, \mathbf{x}_{t-1})$ via SfM or prior models such as MAST3R. In that sense, $r_q(\cdot)$ can be considered as ‘black-box’ function without gradient information, which means that conventional gradient-based solvers may not be applicable. Also note that evaluating $r_q(\mathbf{x}; \mathbf{x}_1, \dots, \mathbf{x}_{t-1})$ for all $\mathbf{x} \in \mathcal{X}$ may be intractable when the set \mathcal{X} is large. This motivates the use of surrogate modeling to optimize the black-box function $r_q(\cdot)$ as delineated next.

4.1. Gaussian process based surrogate model for black-box optimization

Without analytic expression of $r_q(\cdot)$, a surrogate model can be used to estimate r_q at each slot t using all past observations. Hinging on this surrogate model, an acquisition function (AF) is adopted to find \mathbf{x}_t^* at each slot t , which is easy to optimize. While there exist several choices for surrogate modeling, in the present work we will utilize the so-called Gaussian processes (GPs) that can estimate a non-linear function along with its probability density function in a data-efficient manner [21].

At slot $t + 1$, the goal is to find \mathbf{x}_{t+1}^* given the training set $\mathcal{D}_t := \{(\mathbf{x}_\tau, y_\tau)\}_{\tau=1}^t$ for the GP surrogate model consisting of all previous t camera poses collected at $\mathbf{X}_t := [\mathbf{x}_1, \dots, \mathbf{x}_t]^\top$ along with the corresponding (possibly noisy) black-box function evaluations $\mathbf{y}_t := [y_1, \dots, y_t]^\top$. Here $y_\tau = r_q(\mathbf{x}_\tau; \mathbf{x}_1, \dots, \mathbf{x}_{\tau-1}) + n_\tau (\forall \tau)$ and $n_\tau \sim \mathcal{N}(0, \sigma_n^2)$ denotes Gaussian noise uncorrelated across τ . Surrogate modeling with GPs deems the sought objective function $r_q(\cdot)$ as random and assumes that it is drawn from a GP prior. This means that the random vector $\mathbf{r}_t := [r_q(\mathbf{x}_1), r_q(\mathbf{x}_2; \mathbf{x}_1), \dots, r_q(\mathbf{x}_t; \mathbf{x}_1 \dots \mathbf{x}_{t-1})]^\top$ containing all function evaluations up until slot t , is Gaussian distributed as $p(\mathbf{r}_t | \mathbf{X}_t) = \mathcal{N}(\mathbf{0}_t, \mathbf{K}_t) (\forall t)$ where \mathbf{K}_t is the covariance matrix whose (τ, τ') entry is $[\mathbf{K}_t]_{\tau, \tau'} = \text{cov}(r_q(\mathbf{x}_\tau; \mathbf{x}_1, \dots, \mathbf{x}_{\tau-1}), r_q(\mathbf{x}_{\tau'}; \mathbf{x}_1, \dots, \mathbf{x}_{\tau'-1}))$ [21].

In this setting, the black box function r_q is time-varying since it depends at each slot on all previous camera poses and views collected so far. To capture this dynamic behavior of r_q , the covariance between two distinct function evaluations at \mathbf{x}_τ and $\mathbf{x}_{\tau'}$ is modeled as $\text{cov}(r_q(\mathbf{x}_\tau; \mathbf{x}_1, \dots, \mathbf{x}_{\tau-1}), r_q(\mathbf{x}_{\tau'}; \mathbf{x}_1, \dots, \mathbf{x}_{\tau'-1})) = \kappa(\mathbf{x}_\tau, \mathbf{x}_{\tau'}, \tau, \tau')$ where the kernel function $\kappa(\mathbf{x}_\tau, \mathbf{x}_{\tau'}, \tau, \tau')$ is decomposed as

$$\kappa(\mathbf{x}_\tau, \mathbf{x}_{\tau'}, \tau, \tau') = \kappa_s(\mathbf{x}_\tau, \mathbf{x}_{\tau'}) \cdot \kappa_{\text{time}}(\tau, \tau') \quad (6)$$

with $\kappa_s(\mathbf{x}_\tau, \mathbf{x}_{\tau'})$ measuring the pairwise similarity between the camera poses \mathbf{x}_τ and $\mathbf{x}_{\tau'}$, and $\kappa_{\text{time}}(\tau, \tau')$ quantifying the distance between slots τ and τ' with time-decaying behavior. This means that $\kappa_{\text{time}}(\tau, \tau')$ becomes smaller as the distance between τ and τ' becomes larger, which implies that the function evaluations $r_q(\mathbf{x}_\tau; \mathbf{x}_1, \dots, \mathbf{x}_{\tau-1}), r_q(\mathbf{x}_{\tau'}; \mathbf{x}_1, \dots, \mathbf{x}_{\tau'-1})$ are



Figure 3. Visual comparison of ActiveInitSplat with the passive selection counterparts in real-world datasets. For each dataset, we illustrate a single indicative test image where the differences are shown with the annotated yellow dashed boxes. When using ActiveInitSplat, the rendered images are closer to the ground-truth ones.

highly correlated when τ is not far away from τ' . The intuition is that the selection of camera poses and corresponding views should depend more on the most recent observations compared to the oldest ones since the most recent observations carry the information of more collected camera views.

With the GP prior at hand, it can be shown that the posterior pdf of r_q for any (unseen) view $\mathbf{x} \in \mathcal{X}$ at slot $t + 1$ is Gaussian distributed as $p(r_q(\mathbf{x})|\mathcal{D}_t) = \mathcal{N}(\mu_t(\mathbf{x}), \sigma_t^2(\mathbf{x}))$ with mean and variance expressed analytically as [21]

$$\mu_{t+1}(\mathbf{x}) = \mathbf{k}_{t+1}^\top(\mathbf{x})(\mathbf{K}_t + \sigma_n^2 \mathbf{I}_t)^{-1} \mathbf{y}_t \quad (7a)$$

$$\sigma_{t+1}^2(\mathbf{x}) = \kappa(\mathbf{x}, \mathbf{x}, t + 1, t + 1) - \mathbf{k}_{t+1}^\top(\mathbf{x})(\mathbf{K}_t + \sigma_n^2 \mathbf{I}_t)^{-1} \mathbf{k}_{t+1}(\mathbf{x}) \quad (7b)$$

where $\mathbf{k}_{t+1}(\mathbf{x}) := [\kappa(\mathbf{x}_1, \mathbf{x}, 1, t + 1), \dots, \kappa(\mathbf{x}_t, \mathbf{x}, t, t + 1)]^\top$. The mean in (7a) provides a point estimate of the function evaluation at \mathbf{x} and the variance in (7b) quantifies

the associated uncertainty. Relying on the surrogate model $p(r_q(\mathbf{x})|\mathcal{D}_t)$, the next optimal camera pose \mathbf{x}_{t+1}^* is identified optimizing the AF $\alpha(\mathbf{x}|\mathcal{D}_t)$. Here, the camera pose at slot $t + 1$ is selected solving the optimization problem

$$\mathbf{x}_{t+1} = \arg \max_{\mathbf{x} \in \mathcal{X}} \alpha(\mathbf{x}|\mathcal{D}_t) := \mu_{t+1}(\mathbf{x}) \quad (8)$$

where it is intuitive that if the surrogate model captures well the objective function, then selecting \mathbf{x} that maximizes the posterior mean in (7a) most likely provides the maximum of r_q at this slot. Upon selecting \mathbf{x}_{t+1} , the corresponding (possibly noisy) function evaluation y_{t+1} is obtained, and the training set for the surrogate model is augmented as $\mathcal{D}_{t+1} = \mathcal{D}_t \cup \{(\mathbf{x}_{t+1}, y_{t+1})\}$ for the next iteration. This process is repeated up until slot T , as depicted in Fig. 2. Then, the informative set of the T collected camera poses and views can be used for initialization and training of dif-

Scene	Method	r_q value \uparrow	LPIPS \downarrow	SSIM \uparrow	PSNR \uparrow
bonsai	3DGS-passive-random	25.66652	0.3565	0.5672	18.796
	3DGS-passive-standard	27.83765	0.3108	0.6089	18.808
	ActiveInitSplat	35.43626	0.2563	0.7221	22.602
flowers	3DGS-passive-random	1.05133	0.4619	0.3104	14.628
	3DGS-passive-standard	1.51089	0.4606	0.3084	15.318
	ActiveInitSplat	2.58819	0.4025	0.4191	17.538
bicycle	3DGS-passive-random	0.4453	0.4402	0.3775	15.714
	3DGS-passive-standard	0.79184	0.4313	0.3841	17.176
	ActiveInitSplat	0.97178	0.4287	0.4157	17.871
treehill	3DGS-passive-random	0.14839	0.3669	0.5392	16.847
	3DGS-passive-standard	0.15071	0.3699	0.5454	17.077
	ActiveInitSplat	0.17711	0.3649	0.5893	18.023
garden	3DGS-passive-random	20.36397	0.1699	0.7446	24.031
	3DGS-passive-standard	26.13629	0.2070	0.6587	22.772
	ActiveInitSplat	26.9456	0.1678	0.7536	24.384
corn	3DGS-passive-random	0.00314	0.49	0.756	18.88
	3DGS-passive-standard	0.00404	0.456	0.77	20.3
	ActiveInitSplat	0.00409	0.431	0.792	21.649

Table 1. r_q , LPIPS, SSIM and PSNR values for all competing methods on real-world 3D scenes using COLMAP for PC generation in the view selection process for GS.

ferent GS models.

5. Numerical Evaluation

This section demonstrates the merits of the advocated ActiveInitSplat with conducted numerical tests on simulated and real-world datasets.

5.1. Implementation details

The rendering performance of ActiveInitSplat for NVS is initially assessed on real-world datasets including a suite of 3D scenes from the database in [2] and the corn dataset representing a scene of a corn plant inside a lab. Specifically, the ‘bonsai’, ‘flowers’, ‘bicycle’, ‘treehill’, and ‘garden’ from [2] comprise in total $M = 292, 173, 194, 141, 185$ images respectively, and the ‘corn’ dataset consists of $M = 77$ images. To evaluate the generalization rendering performance on unseen novel views, $N_{\text{test}} = 20$ out of the total M images are used for testing, and in our experimental setting the remaining $M - N_{\text{test}}$ images are considered as candidate views, from which $T < M - N_{\text{test}}$ are actively selected from ActiveInitSplat. For the bonsai, flowers, bicycle, and garden datasets ActiveInitSplat is run for $T = 70$ iterations, whereas for the treehill and corn datasets we consider $T = 60$ and $T = 30$ respectively, since the latter datasets comprise in total a smaller number of images compared to the former ones.

In these datasets, we assume access to the poses of the candidate views, whose estimate is already provided by COLMAP [22] in the database [2]; though other pose-

estimation techniques can be utilized such as [14]. It is worth noticing that in practical settings, ActiveInitSplat does not require to be confined to a finite set of candidate views. Specifically, it can identify the most informative ground-truth pose \mathbf{x}_t at each slot t of the active selection process, searching at the entire 3D space that the scene of interest belongs to, instead of being confined to a (possibly limited) set of candidate views. In the next subsection, we will additionally present a realistic ablation study on a simulated environment where ActiveInitSplat can select at each iteration any camera view in the 3D space. For proper evaluation, ActiveInitSplat is tested for five different test sets of $N_{\text{test}} = 20$ independently. In each independent run, T views are actively selected from the remaining $M - N_{\text{test}}$ candidate views. The final evaluation considers the average rendering performance across all five runs. The latter is quantified using the LPIPS, SSIM, and PSNR metrics that are widely adopted for NVS performance assessment. The active selection process of ActiveInitSplat is compared against two passive view selection approaches used for GS; that is (i) ‘3DGS-passive-standard’ that selects views sequentially in the standard way each dataset is constructed (typically following a ‘circular’ formation of collecting images), and (ii) ‘3DGS-passive-random’ that randomly selects a view from the (remaining) candidate views at each iteration. To avoid overstating the benefits of the advocated active selection process, ‘3DGS-Passive-random’ considers the best performing of five independent runs. The training of 3DGS relies on the L1 and D-SSIM loss function as in [12], and is

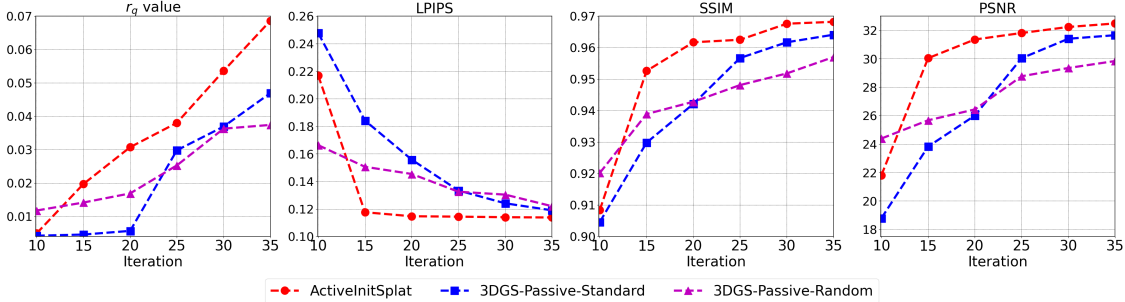


Figure 4. The value of (a) r_q function, (b) LPIPS, (c) SSIM, and (d) PSNR at each iteration of the selection process for all competing methods in the simulated ‘office 4’ environment [24] where any viewpoint in the 3D space can be selected at each iteration. After 10 iterations, the active selection process of ActiveInitSplat results in higher quality 3D scene representation compared to baselines, along with superior GS rendering performance. In addition, ActiveInitSplat converges faster to the desired rendering performance.

Scene	Method	r_q value \uparrow	LPIPS \downarrow	SSIM \uparrow	PSNR \uparrow
bonsai	3DGS-passive-random	26.913	0.4652	0.5829	15.796
	3DGS-passive-standard	105.711	0.4231	0.5562	16.033
	ActiveInitSplat	173.865	0.4120	0.6041	18.121
garden	3DGS-passive-random	29.295	0.5677	0.3606	17.708
	3DGS-passive-standard	27.851	0.5518	0.3382	17.654
	ActiveInitSplat	47.723	0.5348	0.3878	17.806
corn	3DGS-passive-random	1.368	0.4940	0.7770	20.203
	3DGS-passive-standard	1.392	0.4942	0.7787	20.452
	ActiveInitSplat	1.58	0.4916	0.7811	20.584

Table 2. r_q , LPIPS, SSIM, and PSNR values for all competing methods on three indicative real-world 3D scenes using the MAST3R model for PC generation within the view selection process for GS in sparse-view settings.

carried out using 30000 iterations for all datasets except the corn that is trained for 10000 iterations.

For demonstration purposes, the 3D representation $\mathcal{P}_C(\mathbf{x}_t; \mathbf{x}_1, \dots, \mathbf{x}_{t-1})$ used for the black-box function evaluation $r_q(\mathbf{x}_t; \mathbf{x}_1 \dots \mathbf{x}_{t-1})$ upon acquiring \mathbf{x}_t at slot t , is estimated using COLMAP [22] similarly as in the traditional SfM-based GS model in [12]. However, we note that other alternative techniques for obtaining $\mathcal{P}_C(\cdot)$ from 2D images can be readily integrated into our ActiveInitSplat framework; see e.g. a related ablation study in 5.2. For the Gaussian process surrogate model, the kernel functions κ_s, κ_t used for computing κ in (6) are selected to be RBF kernels, which is a typical choice across different GP-based tasks [21]. The kernel hyperparameters are estimated maximizing the marginal likelihood using the *sklearn* package and are re-fitted at the end of each iteration where a newly acquired (\mathbf{x}_t, y_t) pair of camera-view and (noisy) function evaluation becomes available. Note that the kernel function has a significant role in the GP surrogate model and existing works aim to learn the proper kernel form; see e.g. [6, 16, 17, 28], that could be applied in our ActiveInitSplat but exceeds the scope of the current work.

5.2. Numerical results

To assess the performance of ActiveInitSplat in the 3D scenes described in subsection 5.1, the first step is to corroborate the effectiveness of ActiveInitSplat in identifying camera views from diverse viewpoints that provide high-quality 3D scene representation with increased scene coverage. To that end, Table 1 initially demonstrates the r_q function value of all competing methods, that quantifies the quality of a point cloud in terms of density and scene coverage given a specific set of camera views (c.f. section 4). It can be seen in Table 1 that ActiveInitSplat attains a higher r_q value compared to the passive selection counterparts in all datasets illustrating the effectiveness of the proposed GP-based black-box optimization technique in actively capturing informative camera views. With the selection of informative 2D images granted, the goal next is to evaluate how this active selection translates into the GS rendering performance for NVS. Table 1 additionally reports the LPIPS, SSIM, and PSNR rendering metrics for all different methods upon completing T iterations of the selection process. It is evident that ActiveInitSplat is the best-performing approach in all datasets and in all rendering

metrics implying that the passive methods require a denser selection of images to meet the rendering performance of ActiveInitSplat. Besides quantitative evaluations, Fig. 3 also shows qualitative results of indicative rendered test images compared to the corresponding ground-truth ones in all tested 3D scenes. The annotated dashed yellow boxes in Fig. 3 indicate the differences in the rendered images between all competing methods where it is shown that the rendered images from ActiveInitSplat are closer to the ground-truth ones compared to the passive baselines. Next, we present a number of ablation studies to further highlight the merits of ActiveInitSplat.

A.S.1. *How does ActiveInitSplat perform in realistic settings with no constraint on candidate views, i.e. where any viewpoint in the 3D space of interest can be selected?*

To assess ActiveInitSplat in realistic settings where any viewpoint in the 3D space of interest can be selected, we leverage the simulated 3D environment representing the ‘office 4’ scene from [24], where images are rendered using the PyRender software [18]. In this setting, $N_{\text{test}} = 50$ test views are considered to evaluate the generalization rendering performance on unseen novel views. At each iteration t of the view selection process, the proposed approach can actively select any camera pose \mathbf{x}_t in the 3D space of the simulated environment and collect the corresponding RGB view \mathbf{I}_t . For the ‘3DGS_Passive_Standard’ method, images are selected incrementally following a circular path at a fixed height. Note that in this ablation study we also aim to show that ActiveInitSplat converges faster to the desired rendering performance compared to the passive counterparts. To that end, Fig. 4 illustrates the r_q function value along with the LPIPS, SSIM, and PSNR values at every 5 iterations of the camera view selection process for all competing methods. It can be observed that after 10 iterations, ActiveInitSplat enjoys higher r_q function score compared to the passive baselines, leading to higher-quality 3D representations from a more diverse set of camera views. It is worth mentioning that ‘3DGS-Passive-Random’ outperforms ActiveInitSplat in the 10th iteration because its reported result corresponds to the best-performing run among five independent trials, increasing the likelihood of capturing a more informative set of images when only ten are collected. Regarding rendering performance on test views, Fig. 4 clearly shows that after 10 iterations, ActiveInitSplat outperforms all other approaches across all iterations for the LPIPS, SSIM, and PSNR metrics, as anticipated from its higher r_q values. It is also evident that ActiveInitSplat has much faster convergence to the best value compared to the passive selection baselines for all three metrics. For instance, in the LPIPS metric, ActiveInitSplat reaches a lower LPIPS value by iteration 15, whereas both passive baselines require 35 iterations to achieve a comparable result.

A.S.2. *How does ActiveInitSplat perform when (i) alterna-*

tive methods (other than COLMAP) are used to generate $\mathcal{P}_C(\cdot)$ in the optimization process, and (ii) only a limited number of training images are acquired during the active selection process?

Here, the goal is to show the ability of ActiveInitSplat in efficiently integrating alternative COLMAP-free approaches for PC generation within the active view selection process, while accounting for practical settings where only a limited number of training images can be acquired. To that end, we leverage the pre-trained MAST3R model [14] for 3D point cloud generation, in a similar way as in the sparse-view based GS model in [7]. Specifically, the r_q function at each iteration incorporates the MAST3R-generated $\mathcal{P}_C(\cdot)$ and we set the total number of iterations to be 12 to accommodate sparse-view settings. For the experimental evaluation again we consider five different test sets of 20 images and report the average performance. Table 2 presents the LPIPS, SSIM, and PSNR rendering metrics of ActiveInitSplat compared to passive baselines on three indicative real-world datasets for 3DGS utilizing MAST3R-based Gaussian initialization. The results clearly indicate that ActiveInitSplat outperforms passive counterparts, highlighting its effectiveness in integrating alternative, efficient COLMAP-free point cloud generation techniques into the active view selection process. This demonstrates that ActiveInitSplat not only alleviates the computational burden of passive GS with densely collected images but also enhances GS models under sparse-view conditions. It is also worth noting that while MAST3R produces a significantly denser point cloud than COLMAP for GS initialization with only a few images, the sparsity of views may still degrade GS rendering performance. In contrast, a larger training set from COLMAP with *diverse* viewpoints, as captured by our ActiveInitSplat, can lead to improved results.

6. Conclusions

The present work introduces ‘ActiveInitSplat’, a novel approach for actively selecting camera views to capture informative training images, assisting both the initialization and training of GS models. In contrast to existing GS methods that rely on passively pre-selected training images, the proposed framework dynamically acquires 2D images, optimizing density and occupancy-based criteria of the constructed PC from these images. By actively selecting images from diverse viewpoints, ActiveInitSplat ensures comprehensive scene coverage and properly initializes Gaussian functions, conforming them to the ground-truth 3D structure. Numerical tests conducted on both simulated and well-established benchmark datasets highlight the significant advantages of the proposed active selection strategy over conventional passive selection approaches commonly used in existing GS methods.

References

- [1] Jonathan T Barron, Ben Mildenhall, Matthew Tancik, Peter Hedman, Ricardo Martin-Brualla, and Pratul P Srinivasan. Mip-nerf: A multiscale representation for anti-aliasing neural radiance fields. In *Proceedings of the IEEE/CVF International conference on Computer Vision*, pages 5855–5864, 2021. 2
- [2] Jonathan T. Barron, Ben Mildenhall, Dor Verbin, Pratul P. Srinivasan, and Peter Hedman. Mip-nerf 360: Unbounded anti-aliased neural radiance fields. *Proceedings of the IEEE/CVF Conference on Computer Vision and Pattern Recognition*, 2022. 6
- [3] Gaurav Chaurasia, Sylvain Duchene, Olga Sorkine-Hornung, and George Drettakis. Depth synthesis and local warps for plausible image-based navigation. *ACM Transactions on Graphics (TOG)*, 32(3):1–12, 2013. 2
- [4] Anpei Chen, Zexiang Xu, Andreas Geiger, Jingyi Yu, and Hao Su. Tensorf: Tensorial radiance fields. In *Proceedings of European Conference on Computer Vision*, pages 333–350. Springer, 2022. 2
- [5] Liyan Chen, Huangying Zhan, Kevin Chen, Xiangyu Xu, Qingan Yan, Changjiang Cai, and Yi Xu. Activegamer: Active gaussian mapping through efficient rendering. *arXiv preprint arXiv:2501.06897*, 2025. 3
- [6] David Duvenaud, James Lloyd, Roger Grosse, Joshua Tenenbaum, and Ghahramani Zoubin. Structure discovery in nonparametric regression through compositional kernel search. In *Proceedings of the International Conference on Machine Learning*, pages 1166–1174. PMLR, 2013. 7
- [7] Zhiwen Fan, Kairun Wen, Wenyan Cong, Kevin Wang, Jian Zhang, Xinghao Ding, Danfei Xu, Boris Ivanovic, Marco Pavone, Georgios Pavlakos, et al. Instantsplat: Sparse-view sfm-free gaussian splatting in seconds. *arXiv preprint arXiv:2403.20309*, 2024. 2, 3, 8
- [8] Yang Fu, Sifei Liu, Amey Kulkarni, Jan Kautz, Alexei A Efros, and Xiao-long Wang. Colmap-free 3d gaussian splatting. In *Proceedings of the IEEE/CVF Conference on Computer Vision and Pattern Recognition*, pages 20796–20805, 2024. 2
- [9] Armin Hornung, Kai M Wurm, Maren Bennewitz, Cyrill Stachniss, and Wolfram Burgard. Octomap: An efficient probabilistic 3d mapping framework based on octrees. *Autonomous Robots*, 34:189–206, 2013. 4
- [10] Kaiwen Jiang, Yang Fu, Mukund Varma T, Yash Belhe, Xiaolong Wang, Hao Su, and Ravi Ramamoorthi. A construct-optimize approach to sparse view synthesis without camera pose. In *ACM SIGGRAPH 2024 Conference Papers*, pages 1–11, 2024. 2
- [11] Liren Jin, Xingguang Zhong, Yue Pan, Jens Behley, Cyrill Stachniss, and Marija Popović. Activegs: Active scene reconstruction using gaussian splatting. *arXiv preprint arXiv:2412.17769*, 2024. 3
- [12] Bernhard Kerbl, Georgios Kopanas, Thomas Leimkühler, and George Drettakis. 3d gaussian splatting for real-time radiance field rendering. *ACM Transactions on Graphics*, 42(4):139–1, 2023. 1, 2, 3, 6, 7
- [13] Georgios Kopanas, Julien Philip, Thomas Leimkühler, and George Drettakis. Point-based neural rendering with per-view optimization. In *Computer Graphics Forum*, pages 29–43. Wiley Online Library, 2021. 2
- [14] Vincent Leroy, Yohann Cabon, and Jérôme Revaud. Grounding image matching in 3d with mast3r. In *Proceedings of the European Conference on Computer Vision*, pages 71–91. Springer, 2024. 3, 6, 8
- [15] Yuetao Li, Zijia Kuang, Ting Li, Guyue Zhou, Shaohui Zhang, and Zike Yan. Activesplat: High-fidelity scene reconstruction through active gaussian splatting. *arXiv preprint arXiv:2410.21955*, 2024. 3
- [16] Qin Lu, Konstantinos D Polyzos, Bingcong Li, and Georgios B Giannakis. Surrogate modeling for bayesian optimization beyond a single gaussian process. *IEEE Transactions on Pattern Analysis and Machine Intelligence*, 45(9):11283–11296, 2023. 7
- [17] Gustavo Malkomes, Charles Schaff, and Roman Garnett. Bayesian optimization for automated model selection. *Proceedings of Advances in Neural Information Processing Systems*, 29, 2016. 7
- [18] Matthew Matl. Pyrender. <https://github.com/mmatl/pyrender>, 2019. 8
- [19] Manasi Muglikar, Zichao Zhang, and Davide Scaramuzza. Voxel map for visual slam. In *2020 IEEE International Conference on Robotics and Automation (ICRA)*, pages 4181–4187. IEEE, 2020. 4
- [20] Thomas Müller, Alex Evans, Christoph Schied, and Alexander Keller. Instant neural graphics primitives with a multiresolution hash encoding. *ACM Transactions on Graphics (TOG)*, 41(4):1–15, 2022. 2
- [21] Carl Edward Rasmussen and Christopher KI Williams. *Gaussian processes for machine learning*. MIT press Cambridge, MA, 2006. 4, 5, 7
- [22] Johannes Lutz Schönberger and Jan-Michael Frahm. Structure-from-motion revisited. In *Proceedings of the IEEE/CVF Conference on Computer Vision and Pattern Recognition (CVPR)*, 2016. 3, 6, 7
- [23] Brandon Smart, Chuanxia Zheng, Iro Laina, and Victor Adrian Prisacariu. Splatt3r: Zero-shot gaussian splatting from uncalibrated image pairs. *arXiv preprint arXiv:2408.13912*, 2024. 3
- [24] Julian Straub, Thomas Whelan, Lingni Ma, Yufan Chen, Erik Wijmans, Simon Green, Jakob J. Engel, Raul Mur-Artal, Carl Ren, Shobhit Verma, Anton Clarkson, Mingfei Yan, Brian Budge, Yajie Yan, Xiaqing Pan, June Yon, Yuyang Zou, Kimberly Leon, Nigel Carter, Jesus Briales, Tyler Gillingham, Elias Mueggler, Luis Pesqueira, Manolis Savva, Dhruv Batra, Hauke M. Strasdat, Renzo De Nardi, Michael Goesele, Steven Lovegrove, and Richard Newcombe. The Replica dataset: A digital replica of indoor spaces. *arXiv preprint arXiv:1906.05797*, 2019. 7, 8
- [25] Matthew Strong, Boshu Lei, Aiden Swann, Wen Jiang, Kostas Daniilidis, and Monroe Kennedy III. Next best sense: Guiding vision and touch with fisherf for 3d gaussian splatting. *arXiv preprint arXiv:2410.04680*, 2024. 3
- [26] Wei Sun, Xiaosong Zhang, Fang Wan, Yanzhao Zhou, Yuan Li, Qixiang Ye, and Jianbin Jiao. Correspondence-guided

- sfm-free 3d gaussian splatting for nvs. *arXiv preprint arXiv:2408.08723*, 2024. 3
- [27] Towaki Takikawa, Alex Evans, Jonathan Tremblay, Thomas Müller, Morgan McGuire, Alec Jacobson, and Sanja Fidler. Variable bitrate neural fields. In *ACM SIGGRAPH 2022 Conference Proceedings*, pages 1–9, 2022. 2
- [28] Tong Teng, Jie Chen, Yehong Zhang, and Bryan Kian Hsiang Low. Scalable variational bayesian kernel selection for sparse gaussian process regression. In *Proceedings of the AAAI conference on artificial intelligence*, pages 5997–6004, 2020. 7
- [29] Shuzhe Wang, Vincent Leroy, Yohann Cabon, Boris Chidlovskii, and Jerome Revaud. Dust3r: Geometric 3d vision made easy. In *Proceedings of the IEEE/CVF International conference on Computer Vision*, pages 20697–20709, 2024. 3
- [30] Haolin Xiong, Sairisheek Muttukuru, Rishi Upadhyay, Pradyumna Chari, and Achuta Kadambi. Sparsegs: Real-time 360 $\{\deg\}$ sparse view synthesis using gaussian splatting. *arXiv preprint arXiv:2312.00206*, 2023. 3
- [31] Jiale Xu, Shenghua Gao, and Ying Shan. Freesplatter: Pose-free gaussian splatting for sparse-view 3d reconstruction. *arXiv preprint arXiv:2412.09573*, 2024.
- [32] Zehao Zhu, Zhiwen Fan, Yifan Jiang, and Zhangyang Wang. Fsgs: Real-time few-shot view synthesis using gaussian splatting. In *Proceedings of European Conference on Computer Vision*, pages 145–163. Springer, 2024. 3